

Published in final edited form as:

J Am Chem Soc. 2013 April 10; 135(14): 5298–5301. doi:10.1021/ja401221b.

Electrophilic Fragment-Based Design of Reversible Covalent Kinase Inhibitors

Rand M. Miller[‡], Ville O. Paavilainen, Shyam Krishnan, Iana M. Serafimova[‡], and Jack Taunton^{†,*}

[†]Howard Hughes Medical Institute, Department of Cellular and Molecular Pharmacology, University of California, San Francisco, CA 94158.

[‡]Chemistry and Chemical Biology Graduate Program, University of California, San Francisco, CA 94158.

Abstract

Fragment-based ligand design and covalent targeting of noncatalytic cysteines have been employed to develop potent and selective kinase inhibitors. Here, we combine these approaches, starting with a panel of low-molecular weight, heteroaryl-substituted cyanoacrylamides, which we have previously shown to form reversible covalent bonds with cysteine thiols. Using this strategy, we identified electrophilic fragments with sufficient ligand efficiency and selectivity to serve as starting points for the first reported inhibitors of the MSK1 C-terminal kinase domain. Guided by x-ray co-crystal structures, indazole fragment **1** was elaborated to afford **12** (RMM-46), a reversible covalent inhibitor that exhibits high ligand efficiency and selectivity for MSK/RSK-family kinases. At nanomolar concentrations, **12** blocked activation of cellular MSK and RSK, as well as downstream phosphorylation of the critical transcription factor, CREB.

Fragment-based design is a powerful approach for developing ligands that modulate protein function, including protein kinase inhibitors.^{1–3} This strategy relies on the identification of low-molecular weight compounds (100–300 Da) that form specific interactions with the target protein, often of low affinity ($K_d \sim 0.1$ –1 mM). Despite their low binding affinity, fragments often have higher ligand efficiency than typical high-throughput screening hits, which tend to be of higher molecular weight (>300 Da) and therefore have a higher probability of exhibiting steric clashes and other unfavorable interactions with the ligand binding site.⁴ Elaboration of the initial fragment hits guided by NMR or co-crystal structures affords a ligand that is ideally more potent and selective than the initial fragment, while retaining druglike physical properties.

Covalent bond formation between an electrophilic ligand and a poorly conserved, noncatalytic cysteine is another powerful strategy in drug discovery that has been exploited to enhance potency and selectivity.^{5–7} This is especially true for protein kinases, which are difficult to target selectively due to the high sequence and structural conservation of the active site. A large fraction of the 518 human protein kinases contain a solvent-exposed cysteine within or near the ATP binding site.^{8,9} We recently reported a series of compounds

Corresponding Author, jack.taunton@ucsf.edu.

ASSOCIATED CONTENT

Supporting Information Available: Detailed experimental procedures, synthesis and spectral characterization of compounds, crystallographic statistics and collection parameters. This material is available free of charge via the Internet at <http://pubs.acs.org>.

The authors have filed patent applications on cyanoacrylamide kinase inhibitors (licensed to Principia Biopharma, of which J.T. is a co-founder).

that inhibit the RSK2 C-terminal kinase domain (CTD) by forming a reversible covalent bond with a cysteine (C436) found in only eleven of the 518 human protein kinases (Figure 1A).¹⁰ This reversible covalent interaction is made possible by an α -cyanoacrylamide functionality, which forms β -thioether adducts that eliminate more rapidly than acrylamide-derived adducts due to the decreased pK_a of the α -proton (Figure 1B). We sought to exploit this reversible cysteine-targeting chemistry in the context of fragment-based ligand design.

MSK1 is a close relative of RSK2, possessing two kinase domains and a structurally homologous cysteine in its CTD. Despite this similarity, MSK1 is insensitive to our previously developed RSK inhibitors,¹⁰ most likely because it has a large methionine in the gatekeeper position (Figure 1A). Previous studies have suggested that the MSK1 CTD is essential for intramolecular phosphorylation and activation of the N-terminal kinase domain (NTD),¹¹ which subsequently phosphorylates transcription factors and histone H3.^{12,13} Although MSK1 has been implicated in various cancers,^{14–16} the few known inhibitors bind the NTD and show little discrimination among several other AGC-family kinases, including S6K1, AKT1, PRK2, and ROCK2.¹⁷ No inhibitors of the MSK1 CTD have been reported to date.

In this communication, we describe an electrophilic fragment-based approach to ligand discovery. We have used this approach to develop the first reported inhibitor of the MSK1 CTD. This cyanoacrylamide-based inhibitor is active against closely related MSK/RSK-family kinases, but it is highly selective over NEK2 and PLK1, despite the presence of a homologous cysteine in these kinases.

Whereas our previous study started with a known RSK inhibitor,¹⁰ there was no obvious starting point for the current project. Moreover, it was not at all clear whether low-molecular weight electrophiles would be able to discriminate among different noncatalytic cysteines. To test the feasibility of an electrophilic fragment-based approach, we assembled a panel of ten aldehyde fragments (MW 96–250 Da), all with nitrogen-containing heterocycles that are commonly found in kinase inhibitors. Condensation with cyanoacetamide yielded the corresponding cyanoacrylamides **1–10** (Figure 2). We screened **1–10** against three human kinases, all of which contain a cysteine at the same position: RSK2 (C436), NEK2 (C22), and PLK1 (C67). To mimic intracellular redox conditions, glutathione (GSH, 10 mM) was included in all kinase assays, in addition to ATP (0.1 mM) and a peptide or protein substrate. At a molar excess of one million-fold over the kinase, glutathione also increased the stringency of our screen by acting as a competing nucleophile.

We observed significant potency differences among the ten cyanoacrylamides, with distinct patterns of inhibition noted for each kinase. Isomeric indazoles **1** and **2** and azaindole **8** inhibited RSK2 at submicromolar concentrations and high ligand efficiencies (LE = 0.54, 0.56, and 0.39, respectively; see ref. 18 for ligand efficiency calculation). By contrast, **2** and **8** were significantly less potent against NEK2 and PLK1. Azaindole **9** was selective for PLK1 over the other kinases in this screen, and purine **7** exhibited modest selectivity for NEK2. Mutation of the key cysteine in RSK2 (C436V) conferred >100-fold resistance to all of the cyanoacrylamides with submicromolar potency, suggesting that covalent bond formation is required for potent inhibition (Table S1). Unlike cyanoacrylamide **1**, indazole itself failed to inhibit RSK2 at concentrations below 500 μ M, and indazole-5-carboxaldehyde was weakly active against both wild-type and C436V RSK2 (IC₅₀ ~350 μ M, Figure S1). Collectively, the structure-activity relationships in Table 1 suggest that the free energy of covalent bond formation is highly sensitive to structural differences in the fragments and the cysteine-containing kinase.

To gain structural insight into the extraordinary ligand efficiency of indazole **1**, we determined its co-crystal structure bound to RSK2 (PDB code 4JG6). The structure reveals the same kinase hinge-binding mode observed with other indazole inhibitors,^{19,20} in which the N1 proton donates a hydrogen bond to the carbonyl of L495 while N2 accepts a hydrogen bond from the amide of M496 (Figure 3A). Contiguous electron density was observed between C436 and the β -carbon of the cyanoacrylamide, consistent with covalent bond formation. Notably, indazole **1** does not extend into the hydrophobic pocket behind the gatekeeper T493 (Figure 3A). This observation suggested that, unlike our previously developed RSK2 inhibitors,¹⁰ **1** would be sterically compatible with a bulkier side chain in the gatekeeper position. Consistent with this hypothesis, indazole **1** inhibited the T493M gatekeeper mutant of RSK2 with an IC₅₀ of 230 nM.

A co-crystal structure of azaindole **8** (PDB code: 4JG7) revealed that it binds RSK2 in a completely different manner from **1** (Figure 1B). The electron density for **8** was clear and unambiguous, allowing its accurate placement within the RSK2 active site (Figure S2). Unlike structurally related kinase inhibitors, the azaindole moiety of **8** does not engage the hinge. Rather, the ketone accepts a hydrogen bond from hinge residue M496, while the azaindole projects toward the entrance of the ATP pocket, sandwiched between the side chains of I428, M496 and L546. This interaction is accompanied by a conformational change in the glycine-rich loop, which contains I428 (Figure S3). In both co-crystal structures, the nitrile and amide groups of the covalently bound inhibitors are solvent exposed and poorly resolved, precluding assignment of the newly formed α -stereocenter. Together, the structures suggest that potent RSK2 inhibition by cyanoacrylamide fragments **1** and **8** requires the simultaneous satisfaction of two geometric restraints: at least one hydrogen bond to the hinge and an unstrained covalent bond to C436.

An overlay of the two co-crystal structures suggested that aromatic substituents appended to the 3-position of indazole **1** would fill the hydrophobic cleft occupied by the azaindole moiety of **8** (Figure 3B). We therefore designed and synthesized the trimethoxyphenyl-substituted indazole **11** (Table 2). This provided a 20-fold increase in potency toward RSK2, but its selectivity over NEK2 and PLK1 was poor. Addition of a 1,1-dimethyl-2-hydroxyethyl substituent to the primary amide of **11** afforded our optimized inhibitor **12**, which retained potency against RSK2 and showed increased selectivity over NEK2 and PLK1 (Table 2, Figure 4A). The IC₅₀ of **12** against T493M RSK2 was below 2.5 nM, the lower limit of our assay (LE >0.35).

The selectivity of **12** was further defined by screening a commercial panel of 26 kinases (Table S2), twelve of which have a cysteine at various positions throughout the ATP-binding site (e.g., BTK, EGFR, JAK3, KDR). At a screening concentration of 1 μ M, NEK2 and PLK1 were the only kinases that were significantly inhibited (77% and 84% inhibition, respectively; [ATP] = 200 and 15 μ M). We note that wild-type and T493M RSK2 were >40-fold more sensitive than NEK2 and PLK1 when tested under identical conditions in our laboratory (Table 2 and Figure 4A, 0.1 mM ATP, 10 mM GSH). Kinases showing negligible inhibition by **12** include among others, MEK1, ERK1, and p38 MAPK, all of which are upstream regulators of RSK/MSK-family kinases (Table S2).

A co-crystal structure of **12** bound to T493M RSK2 (PDB code: 4JG8) confirmed the binding mode anticipated by our structural analysis of **1** and **8** (Figure 4B,C). Overlaying the co-crystal structures of **12** and **1** revealed that the indazole cores of both inhibitors were perfectly aligned, with the indazole of **12** packed against the methionine gatekeeper (M493). Similar to the azaindole of **8**, the trimethoxyphenyl substituent of **12** was nestled between the side chains of I428, M496 and L546. The 1,1-dimethyl-2-hydroxyethyl amide group of **12** extended beneath the glycine-rich loop (Figure 4B,C). Given the low sequence

conservation and conformational heterogeneity of this loop,^{21,22} this interaction may account for the improved selectivity of **12** compared to **11** (Table 2). Finally, a covalent bond was observed between C436 and the electrophilic β -carbon of the cyanoacrylamide. Unfolding the **12**/RSK2 complex with guanidinium HCl resulted in the quantitative release of **12**, confirming that the covalent bond is reversible and that its stability requires the intact folded structure of the kinase domain (Figure S4).

The ability of **12** to inhibit T493M RSK2 with more than 1,000-fold higher potency than our previous cyanoacrylamide inhibitors¹⁰ prompted us to test the related kinase, MSK1, which also has a methionine in the gatekeeper position (Figure 1A). To date, it has not been possible to perform kinase assays with the isolated MSK1 CTD. We therefore asked whether **12** could prevent CTD-mediated autophosphorylation of fulllength MSK1 in stimulated cells. Cells expressing HA-tagged MSK1 were treated with increasing concentrations of **12**, followed by stimulation with phorbol myristate acetate (PMA). As revealed by a phospho-specific antibody that recognizes pS376, **12** inhibited MSK1 CTD activity in the context of the full-length protein, with an IC₅₀ of ~100 nM (Figure 4D). In the same cell-based assay format, **12** was equipotent against the closely related kinases, MSK2, RSK2, and RSK3 (Figure S5).

MSK1/2 are among several kinases that have been shown to regulate the cAMP-response element binding transcription factor, CREB, via phosphorylation of S133. Studies with knockout mice have demonstrated a role for MSK1/2 in CREB S133 phosphorylation in response to mitogens (e.g., PMA) and cellular stress (e.g., UV-C).¹³ However, until now, it has not been possible to test whether the CTD of endogenous MSK1/2 is required for CREB phosphorylation. Importantly, **12** was found to be inactive toward several kinases previously shown to phosphorylate CREB, including AKT1, PKA, CAMK2, and PKC θ (Table S2). Treatment of HeLa cells with **12** reduced CREB phosphorylation (IC₅₀ ~300 nM) under both PMA and UV-C stimulation conditions (Figure 4E). By contrast, a potent RSK inhibitor,¹⁰ which is inactive against MSK1/2, failed to block CREB phosphorylation under these conditions (Figure S6). These results indicate that the MSK1/2 CTD plays a critical role in promoting CREB phosphorylation by the NTD.

In this study, we have developed a new approach to fragment-based ligand design that exploits the reversible conjugate addition of thiols to cyanoacrylamides. This chemistry, when deployed against a poorly conserved noncatalytic cysteine, provides enhanced selectivity and potency, while avoiding the formation of irreversible covalent adducts. Indeed, it is not clear that a fragment-based approach would be feasible with electrophiles that form irreversible covalent bonds. Inhibition/binding would occur under kinetic control and would be sensitive to the intrinsic nucleophilicity of a given cysteine.²³ Although intriguing results with acrylamide fragments have been reported,²⁴ it remains to be seen whether useful levels of kinetic discrimination can be achieved.

The structure-activity relationships observed with our collection of 10 cyanoacrylamides suggest that potency is not solely driven by the free energy of covalent bond formation. Rather, specific noncovalent interactions (hinge hydrogen bonds, van der Waals contacts, and steric complementarity) are required in concert with the covalent bond to cooperatively stabilize the complex. Given the geometric restraints imposed by an unstrained thioether bond, it may be possible to computationally predict the binding poses of fragment hits, potentially extending the utility of this approach to cases where experimental structures cannot be obtained. Relative to disulfide-based fragments,²⁵ the cyanoacrylamide electrophile is more compatible with the thiol-rich cellular environment and may therefore be retained during inhibitor optimization for use in biological studies. Finally, we anticipate

that cyanoacrylamide fragments can be applied to cysteine-containing targets beyond kinases, enabling the discovery of new chemical probes.

Supplementary Material

Refer to Web version on PubMed Central for supplementary material.

Acknowledgments

This work was supported by the NIH (GM071434 to J.T.), the Academy of Finland and the Sigrid Juselius Foundation (to V.P.), and the California Tobacco Related Disease Research Program (19FT-0091 to S.K.). We thank Christopher Waddling at the UCSF Crystallography Facility for assistance with instrumentation and software.

REFERENCES

1. Erlanson DA, McDowell RS, O'Brien T. J. Med. Chem. 2004; 47:3363–3482.
2. Howard S, Berdini V, Boulstridge JA, Carr MG, Cross DM, Curry J, Devine LA, Early TR, Fazal L, Gill AL, Heathcote M, Maman S, Matthews JE, McMenamin RL, Navarro EF, O'Brien MA, O'Reilly M, Rees DC, Reule M, Tisi D, Williams G, Vinkovi M, Wyatt PG. J. Med. Chem. 2009; 52:379–388. [PubMed: 19143567]
3. Bamborough P, Brown MJ, Christopher JA, Chung C, Mellor GW. J. Med. Chem. 2011; 54:5131–5143. [PubMed: 21699136]
4. Hann MM, Leach AR, Harper G. J. Chem. Inf. Comput. Sci. 2001; 41:856–864. [PubMed: 11410068]
5. Potashman MH, Duggan ME. J. Med. Chem. 2009; 52:1231–1246. [PubMed: 19203292]
6. Fry DW, Bridges AJ, Denny WA, Doherty A, Greis KD, Hicks JL, Hook KE, Keller PR, Leopold WR, Loo JA, McNamara DJ, Nelson JM, Sherwood V, Smaill JB, Trump-Kallmeyer S, Dobrusin EM. Proc. Natl. Acad. Sci. 1998; 95:12022–12027. [PubMed: 9751783]
7. Hagel M, Niu D, St Martin T, Sheets MP, Qiao L, Bernard H, Karp RM, Zhu Z, Labenski MT, Chaturvedi P, Nacht M, Westlin WF, Petter RC, Singh J. Nat. Chem. Biol. 2011; 7:22–24. [PubMed: 21113170]
8. Zhang J, Yang PL, Gray NS. Nat. Rev. Cancer. 2009; 9:28–39. [PubMed: 19104514]
9. Leproult E, Barluenga S, Moras D, Wurtz JM, Winssinger N. J. Med. Chem. 2011; 54:1347–1355. [PubMed: 21322567]
10. Serafimova IM, Pufall MA, Krishnan S, Duda K, Cohen MS, Maglathlin RL, McFarland JM, Miller RM, Frödin M, Taunton J. Nat. Chem. Biol. 2012; 8:471–476. [PubMed: 22466421]
11. Deak M, Clifton AD, Lucocq JM, Alessi DR. EMBO J. 1998; 17:4426–4441. [PubMed: 9687510]
12. McCoy CE, Campbell DG, Deak M, Bloomberg GB, Arthur JSC. Biochem. J. 2005; 387:507–517. [PubMed: 15568999]
13. Wiggin GR, Soloaga A, Foster JM, Murray-Tait V, Cohen P, Arthur JSC. Mol. Cell. Biol. 2002; 22:2871–2881. [PubMed: 11909979]
14. Odgerel T, Kikuchi J, Wada T, Shimizu R, Kano Y, Furukawa Y. Leukemia. 2010; 24:1087–1090. [PubMed: 20357825]
15. Pérez-Cadahía B, Drobic B, Espino PS, He S, Mandal S, Healy S, Davie JR. J. Biol. Chem. 2010; 286:42–49. [PubMed: 21071437]
16. van der Heide LP, van Dinther M, Moustakas A, ten Dijke P. J. Biol. Chem. 2011; 286:5003–5011. [PubMed: 21106525]
17. Naqvi S, Macdonald A, McCoy CE, Darragh J, Reith AD, Arthur JSC. Biochem. J. 2012; 441:347–357. [PubMed: 21970321]
18. Ligand efficiency is calculated according to ref. 2, with IC₅₀ as a surrogate for K_d at 293 K, using $\Delta G = -RT\ln(IC_{50})$ and $LE = \Delta G / (\# \text{ heavy atoms})$.
19. Zhu G, Gandhi VB, Gong J, Thomas S, Woods KW, Song X, Li T, Diebold RB, Luo Y, Liu X, Guan R, Klinghofer V, Johnson EF, Bouska J, Olson A, Marsh K, Stoll VS, Mamo M, Polakowski

- J, Campbell TJ, Martin RL, Gintant GA, Penning TD, Li Q, Rosenberg SH, Giranda VL. *J. Med. Chem.* 2007; 50:2990–3003. [PubMed: 17523610]
20. McTigue M, Murray BW, Chen JH, Deng -L, Solowiej J, Kania RS. *Proc. Natl. Acad. Sci.* 2012; 109:18281–18269. [PubMed: 22988103]
21. Patel RY, Doerksen RJ. *J. Proteome Res.* 2010; 9:4433–4442. [PubMed: 20681595]
22. Guimarães CRW, Rai BK, Munchof MJ, Liu S, Wang J, Bhattacharya SK, Buckbinder L. *J. Chem. Inf. Model.* 2011; 51:1199–1204. [PubMed: 21568278]
23. Weerapana E, Wang C, Simon GM, Richter F, Khare S, Dillon MBD, Bachovchin DA, Mowen K, Baker D, Cravatt BF. *Nature.* 2010; 468:790–795. [PubMed: 21085121]
24. Nonoo RH, Armstrong A, Mann DJ. *ChemMedChem.* 2012; 7:2082–2086. [PubMed: 23033251]
25. Erlanson DA, Braisted AC, Raphael DR, Randal M, Stroud RM, Gordon EM, Wells JA. *Proc. Natl. Acad. Sci.* 2000; 97:9367–9372. [PubMed: 10944209]

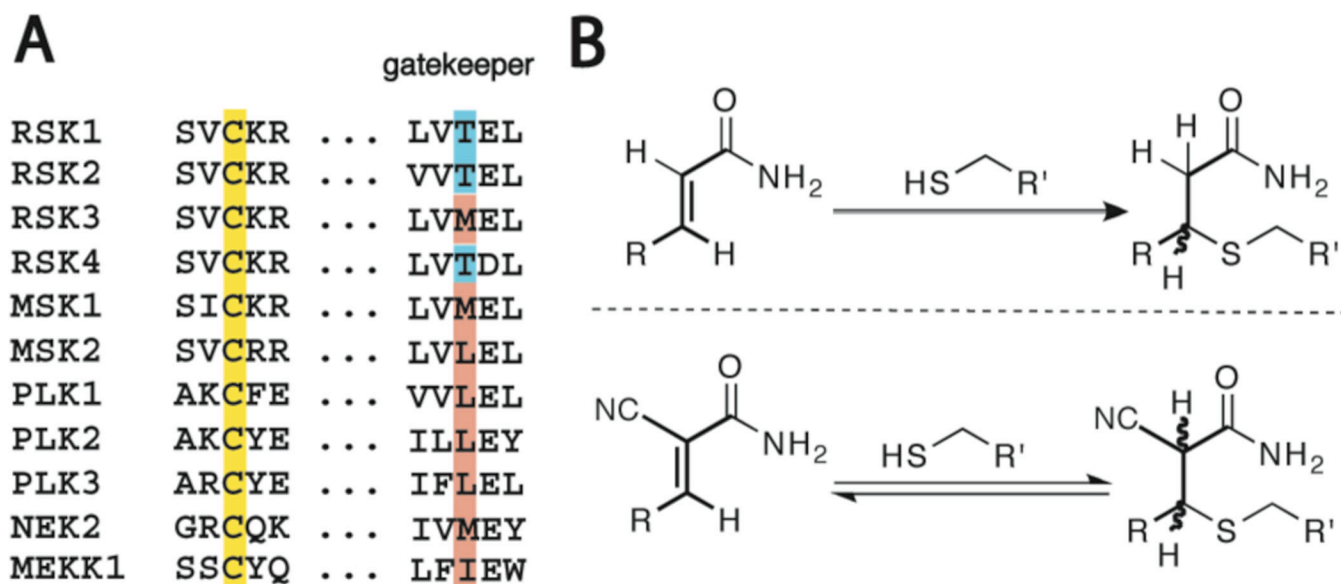


Figure 1.

(A) Sequence alignment of 11 human kinases containing a cysteine at the same position as C436 of RSK2 (yellow). The gatekeeper position is highlighted in blue (threonine) or red (larger hydrophobic residues). (B) Michael adducts of thiols with acrylamides are kinetically stable, whereas cyanoacrylamides form rapidly reversible adducts with thiols.

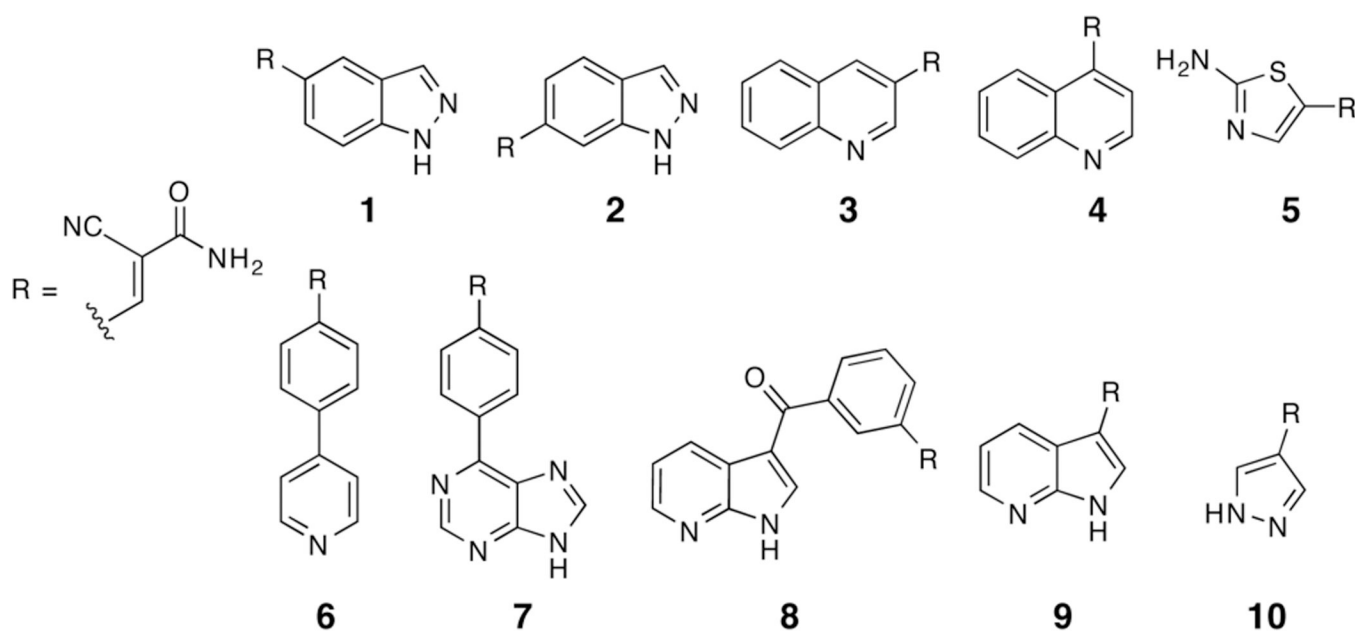


Figure 2.
Cyanoacrylamide-based fragments used in this study.

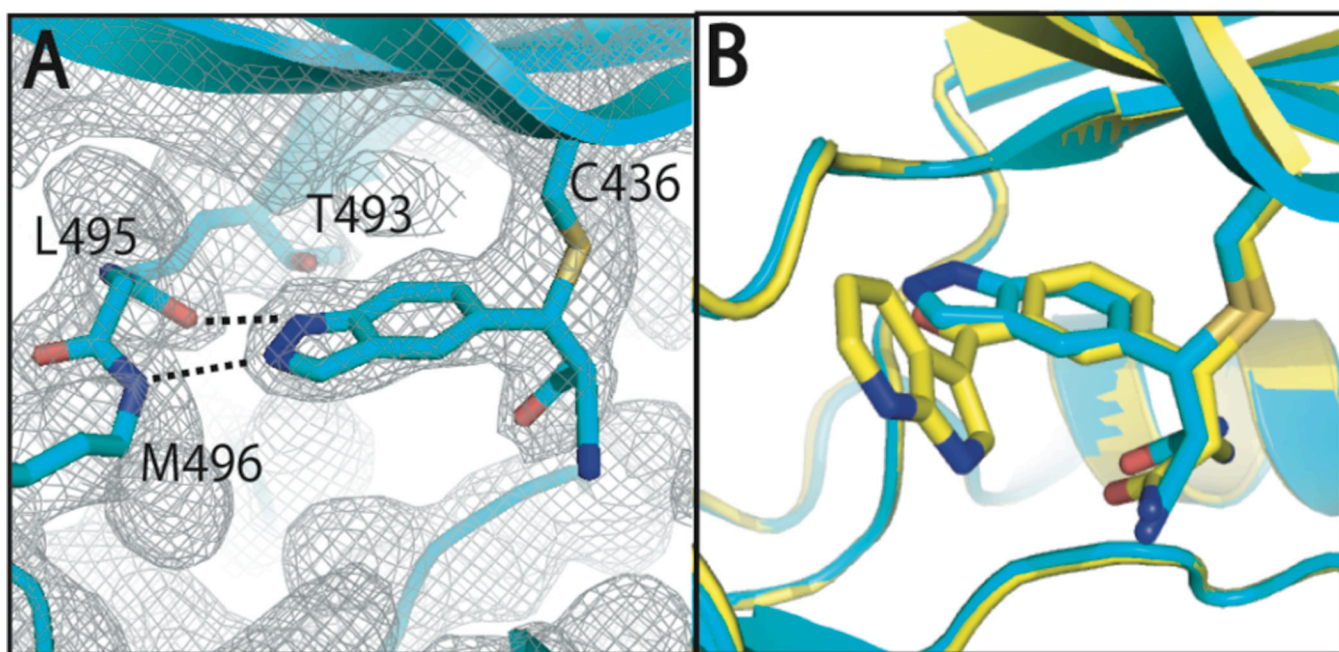
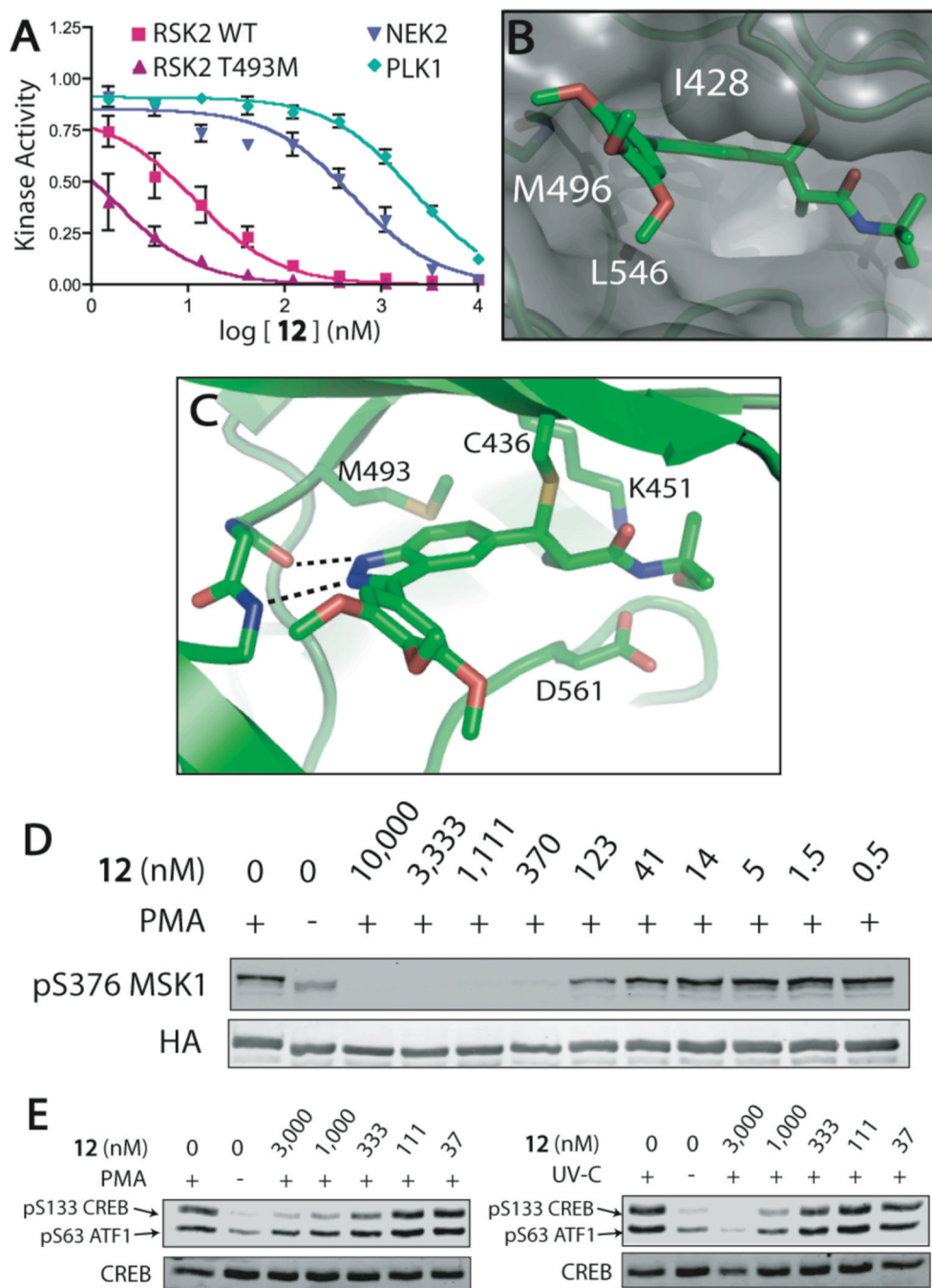


Figure 3.
(A) Co-crystal structure of **1** bound to the RSK2 CTD. $2F_o-F_c$ map is contoured to 1σ . (B) Overlay of the structures of **1** (blue) and **8** (yellow) bound to RSK2, indicating the potential for aryl substitution at the 3-position of the indazole scaffold.

**Figure 4.**

(A) Kinase assay dose-response curves for **12** (mean \pm SD). (B) and (C) Co-crystal structure of **12** bound to T493M RSK2. (D) Inhibition of MSK1 autophosphorylation in stimulated COS7 cells. (E) Inhibition of CREB phosphorylation in HeLa cells after stimulation with PMA or UV-C.

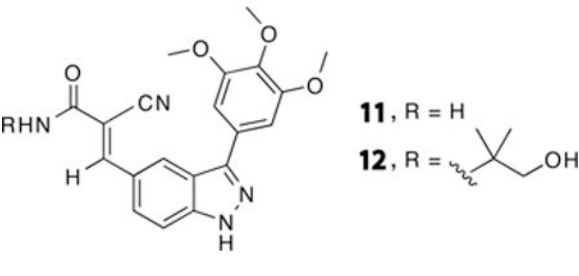
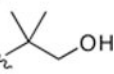
Table 1*In vitro* kinase assay IC₅₀ values (μM)^a

	RSK2	NEK2	PLK1
1	0.36 ± 0.01	1.4 ± 0.2	0.57 ± 0.07
2	0.23 ± 0.01	3.4 ± 0.7	2.5 ± 0.4
3	38 ± 1	14 ± 0.7	37 ± 2
4	1.4 ± 0.1	96 ± 6	25 ± 2
5	21 ± 2	>150	> 300
6	6.0 ± 0.2	6.1 ± 0.5	45 ± 7
7	4.4 ± 0.6	1.1 ± 0.2	27 ± 0.4
8	0.12 ± 0.02	2.1 ± 0.4	> 10
9	8.2 ± 0.3	26 ± 0.2	< 0.62
10	68 ± 3	>100	53 ± 2

^aValues reported as the mean ± range for duplicate measurements.

Table 2

In vitro kinase assay IC₅₀ values (nM) for 11 and 12^a.

 <p>11, R = H 12, R = </p>				
	RSK2	RSK2 T493M	NEK2	PLK1
11	15 ± 2 ^b	3 ± 1	62 ± 8	37 ± 3
12	12 ± 3	< 2.5 ^c	530 ± 16	2200 ± 200

^aValues reported as the mean ± SD (n = 3) unless otherwise noted. All assays contain 10 mM GSH and 100 μM ATP.

^bValue is the mean ± range for duplicate measurements.

^cCalculated IC₅₀ is less than half the concentration of kinase present (5 nM).